Review of current progress in nanometrology with the helium ion microscope

Review of current progress in nanometrology with the helium ion microscope

Michael T Postek[1,3]**, András Vladár**[1]**, Charles Archie**[2]** and Bin Ming**[1]

[1] National Institute of Standards and Technology[4,5], Gaithersburg, MD 20899, USA
[2] IBM, Semiconductor Research and Development Center, Systems and Technology Group, Hopewell Junction, NY 12533, USA

E-mail: postek@nist.gov

Abstract

Scanning electron microscopy has been employed as an imaging and measurement tool for more than 50 years and it continues as a primary tool in many research and manufacturing facilities across the world. A new challenger to this work is the helium ion microscope (HIM). The HIM is a new imaging and metrology technology. Essentially, substitution of the electron source with a helium ion source yields a tool visually similar in function to the scanning electron microscope, but very different in the fundamental imaging and measurement process. The imaged and measured signal originates differently than in the scanning electron microscope and that fact and its single atom source diameter may be able to push the obtainable resolution lower, provide greater depth-of-field and ultimately improve the metrology. Successful imaging and metrology with this instrument entails understanding and modeling of new ion beam/specimen interaction physics. As a new methodology, HIM is beginning to show promise and the abundance of potentially advantageous applications for nanometrology has yet to be fully exploited. This paper discusses some of the progress made at NIST in collaboration with IBM to understand the science behind this new technology.

Keywords: helium ion, microscope, HIM, scanning electron microscope, SEM, nanomanufacturing, nanometrology, critical dimension

1. Introduction

Nanotechnology and the associated nanometrology are pushing current technology to its limits [1–4]. The scanning and transmission electron microscopes have incrementally improved in performance and other scanned probe technologies such as atomic force microscopy, scanning tunneling microscopy and focused ion beam microscopy have all been applied to nanotechnology with various levels of

success. Over the years, the evolution of these technologies has been steady and highly responsive to the needs of the research community.

A new tool for nanotechnology is the scanning helium ion microscope (HIM). As reported in earlier papers [5–10], the HIM is a new approach to imaging and metrology for nanotechnology which may be able to push the current resolution barrier lower and provide new contrast mechanisms (figure 1). This means that the metrology done with this instrument can be better for some materials than for its electron beam instrument counterparts. The HIM also promises the potential for greater depth of field (DOF), new imaging modes and the potential for charge-free imaging at higher landing energies without the need for conductive coating. But, successful imaging and metrology with this instrument entails development of new ion beam/specimen

---

[3] Author to whom any correspondence should be addressed.
[4] Contribution of the National Institute of Standards and Technology, not subject to copyright.
[5] Certain commercial equipment is identified in this report to adequately describe the experimental procedure. Such identification does not imply recommendation or endorsement by the National Institute of Standards and Technology, nor does it imply that the equipment identified is necessarily the best available for the purpose.
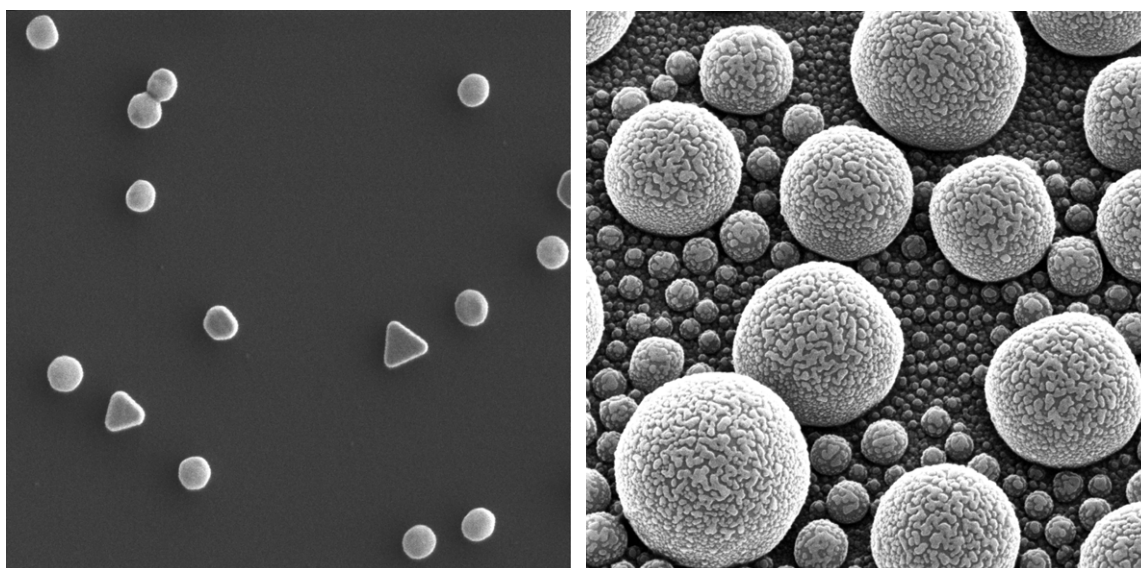
Figure 1. Resolution and depth of field in the helium ion microscope. (Left) 60 nm gold particles (field of view = 1000 nm) and (right) evaporated nickel particles (field of view = 2.5 μm).

interaction physics which is different from the current electron beam interaction models. As a new methodology, HIM is beginning to show promise and the abundance of potentially advantageous applications for nanometrology has yet to be fully exploited.

The National Institute of Standards and Technology (NIST) was fortunate to receive the first commercial HIM [6] and this paper discusses some of the progress made at NIST in collaboration with the IBM Semiconductor Research and Development Center to improve its performance and to understand the science and capabilities of this new instrumentation for dimensional metrology. In addition, it is the NIST goal to understand potential differences between HIM and contemporary scanning electron microscope (SEM) instruments. Clearly, this is a difficult task since the SEM and the HIM appear similar in that both are scanned particle beam instruments but are quite different in their evolutionary state, operational parameters, modeling and state of metrology development.

2. Materials and methods

2.1. Instruments

The scanning helium ion microscopes used in this work were either a Zeiss Orion Plus HIM installed in the NIST Advanced Measurement Laboratory or an engineering instrument installed at the Zeiss/ALIS (see footnote 5) facility in Peabody, MA.

2.2. Sample preparation

No special sample preparation techniques were used for general imaging and metrology. HIM sample preparation is generally similar to that used for standard SEM sample preparation.
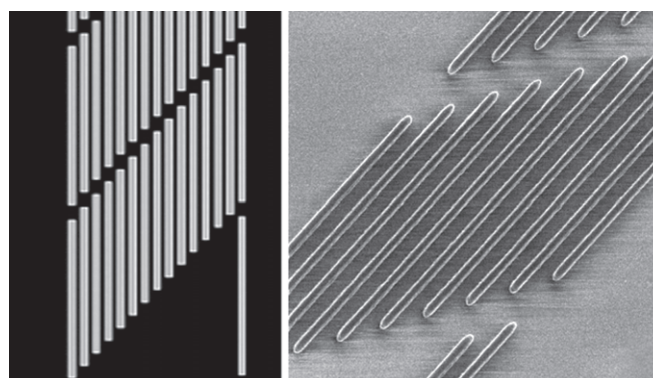

Figure 2. Test structures used in the photoresist studies. (Left) computer aided design of the test structures. (Right) SEM image of the patterned photoresist structures (field of view = 3 μm). This overall pattern is designed for cross section metrology (as described in the text). The nested lines extend for several millimeters on the wafer in order to facilitate cleaving the wafer through the lines.

2.3. Experiments on photoresist patterned silicon wafers

One photoresist system was exposed using a 248 nm deep ultraviolet (DUV) lithography process, while the other used a 193 nm process. Both were chemically amplified resist systems where the total exposure energy dose came from a combination of the photon exposure and a subsequent timed bake at elevated temperature. Both resist systems are known to be affected by modest irradiation, such as that caused by SEM imaging. The same photomask was used for both exposures. Figure 2 (left) shows the computer aided design of the test structure used in the studies and figure 2 (right) is a SEM image of the actual patterned photoresist structures (left). These structures are designed for cross section metrology; the nested lines extend for several millimeters on the wafer in order to facilitate cleaving the wafer through the lines. Diagonal breaks in the lines occur every 5 μm. The linewidth is approximately
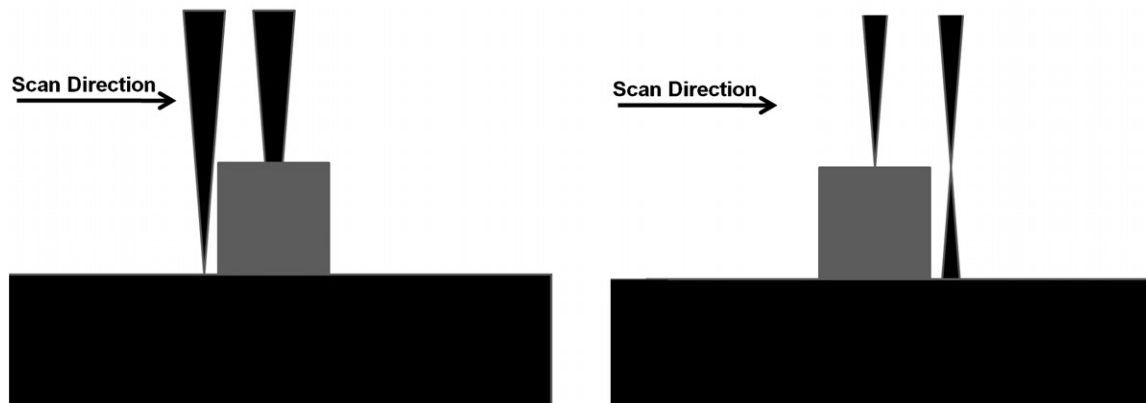
Figure 3. DOF and the effect of beam defocus on imaging and metrology. (Left) beam focused on substrate. The 3D conical electron beam, scanning from left to right, interacts with the leading edge of the structure prior to the focal point. Thus, the signal from the leading edge is summed with the signal from the location of the primary beam interaction. (Right) beam focused on the top of the sample. As the focused beam leaves the sample it is defocused at the substrate. The larger the DOF characteristic of the instrument, the less the impact of this problem.

135 nm. The structures on the wafer offer many similar locations for experimentation. After construction of the wafers and survey by SEM to confirm print quality, the wafers were diced to produce wafer fragments of less than 3 cm^2 which are suitable for insertion into the HIM. Some fragments contained complete versions of the design while others were intentionally cleaved to bisect the structures in order to study in the cross section mode. These experiments were conducted at the Zeiss/ALIS factory in Peabody, MA. The HIM used a 31.5 keV beam with a 10 pA probe current. The HIM uses a mechanical cryocooler to reduce the temperature of the gun down to 72–74 K. During actual scanning, this cooling device was turned off in order to reduce vibrations.

3. Comparison of the scanning electron and helium ion microscopes

3.1. The primary electron and ion beams

The scanning electron microscope and the helium ion microscope share a number of fundamental characteristics. The primary beam in each microscope is composed of a three-dimensional distribution of electrons or ions along and across the beam. The beam is generally thought to have a somewhat double-conical shape. This defines the important half-angle parameter that determines the DOF and the disk of least confusion where the best focus (i.e. the smallest spot size) can be achieved. The small beam convergence angle of the particle beam instruments results in high DOF. Large DOF has always been a positive characteristic of the scanning electron microscope [11], but it can be even more pronounced in the HIM. This is a consequence of the single atom source of the ions with the HIM [12–15]. Under normal operating conditions, this can result in a narrower convergence angle than the SEM (depending upon the instrument operating conditions). Therefore, the overall DOF can be larger than the SEM even at higher magnifications [15]. In certain cases, using the most optimum conditions and instrument settings, the DOF of the HIM can be as much as five times greater than the SEM.

Large DOF is highly desirable. The size of the DOF can have consequences to the metrology with scanned beam systems especially where high-aspect ratio structures are concerned. This relates directly to whether the beam is focused on the top of a structure or the base of the structure and then becomes an important measurement consideration (figure 3). When the particle beam is focused at the substrate, signal may be generated by the beam remotely from the smallest focal spot because a portion of the beam above the surface contacts the structure before the focused part of the beam scans to it (figure 3, left). Conversely, if the beam is focused at the top of a structure (figure 3, right), it will rapidly defocus when it reaches an edge and then be somewhat defocused at the substrate. The larger the DOF, the less this affects the imaging and metrology.

3.2. Excited volume

One of the key issues for nanometrology in any particle beam instrument is the understanding that signal is generated from more than just the initial point of impact of the primary beam. The 'image' is a point-by-point representation of the total signal generated as the beam is scanned across a given sample. Any modification of that signal due to signal generation or collection inefficiency will be mirrored in the imaged or measured data.

Depending upon the particle source, accelerating voltage and materials irradiated, there is a finite volume excited by the primary particle beam. This volume may extend quite deeply into the material. Ideally, the beam would only interact with the surface, but that is not the case. The current understanding is that the volume excited by the primary electron beam in the SEM and the volume excited by the HIM are quite different [6]. Figure 4 illustrates a comparison of modeled electron beam interaction data from the Monte Carlo program CASINO 2.42 [16–18] (left) and ion beam interaction data modeled by SRIM 2008.04 [19] (right). In both of the modeled examples, 30 keV particles are interacting with an infinitely thick silicon (Si) sample. Note the fundamental
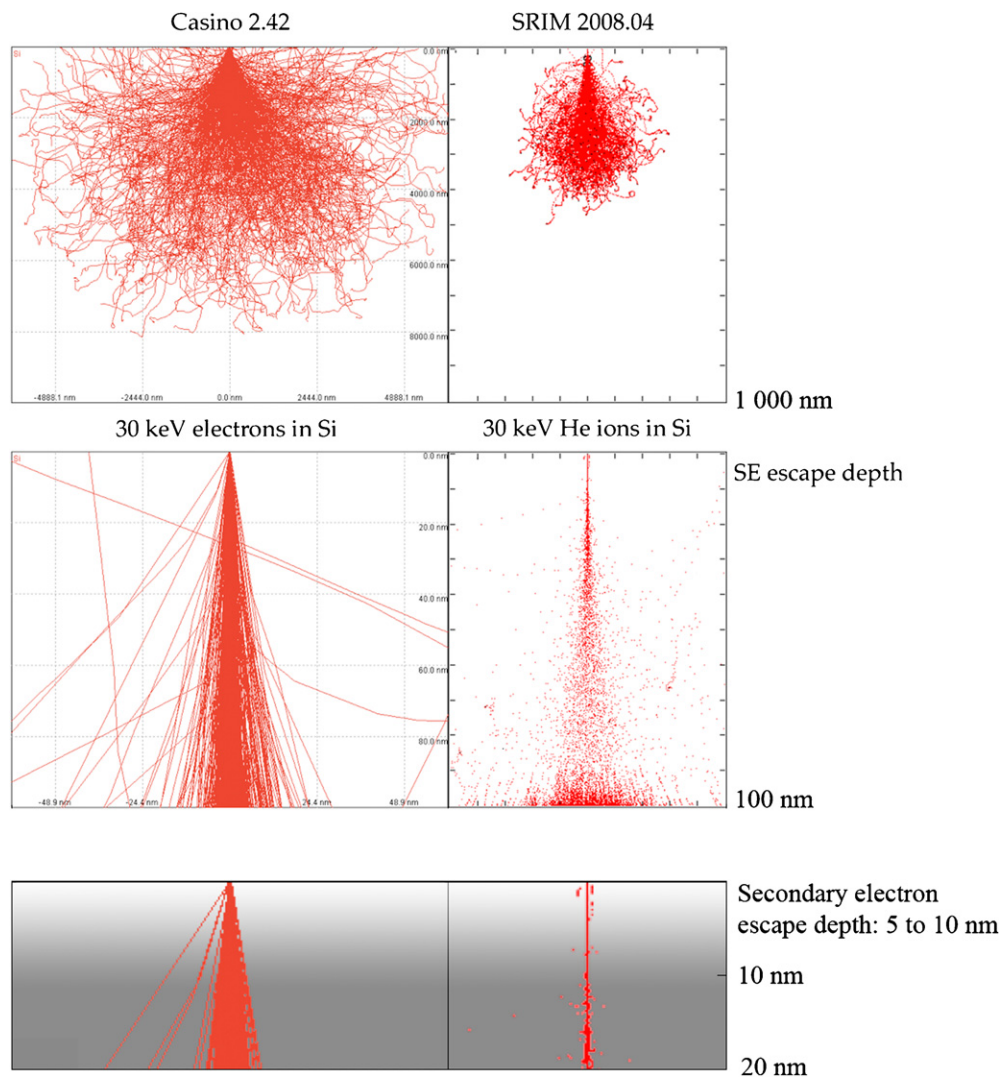
Figure 4. Comparison of the electron beam interaction data from the Monte Carlo program CASINO 2.42 (left) and ion beam interaction data modeled by SRIM 2008.04 (right). In both of the modeled examples, 30 keV particles are interacting with an infinitely thick silicon sample. Note the fundamental difference in the size and depth of the interaction volumes, especially in the top figures.

difference in the interaction volumes especially in the lower comparison. This volume is where the important beam–specimen interactions take place and it has been modeled, as well as, documented experimentally for the SEM [20, 21] but has not been done, as of yet, for the HIM.

Within the excited volume, the secondary electron (SE) escape depth is that region from which the SEs have enough energy to leave the sample surface to be potentially collected. The deeper the SE are generated, the less likely they will escape and be collected. Typically, the escape depth can be a few nanometers to up to more than 10 nm, depending on the sample material. For metals, the depth is shallower; for insulators and biological materials, it is generally larger. The shape and size, the depth reached by electrons and ions and the SE generation efficiency all strongly depend on the landing energy of the electrons or ions and the sample material irradiated. The landing energy of electrons in an SEM is variable; however, adjustable ion acceleration in the HIM is a capability still to be implemented in the NIST HIM (this capability will greatly expand the parameter space for all HIM experiments).

It is clear from model shown in figure 4 (lower) that as the ion beam enters the sample, it scatters far less within the SE escape zone than electrons. The positive consequence of this is that fewer SEs are generated near the surface or remotely from the impact point of the primary ion beam (figure 5). In figure 5, one can readily see that in the SEM, signal can be generated from regions quite a distance from the incident primary beam not just that single point where the primary beam enters the sample. All of the sources of the signal are summed for each pixel of the image collected. Hence, (as discussed below) the SE signal can be recorded from areas of the sample remote from the impact point of the primary beam.

The ion scatter characteristic of the HIM, described above, can also be exploited for extremely fine line lithography. Electron beam lithography (EBL) has been used in lithographic patterning for many years. EBL suffers from many of the same issues as SE imaging such as extraneous exposure from fast SEs and backscattered electrons. Focused ion beam lithography with a gallium source has not been
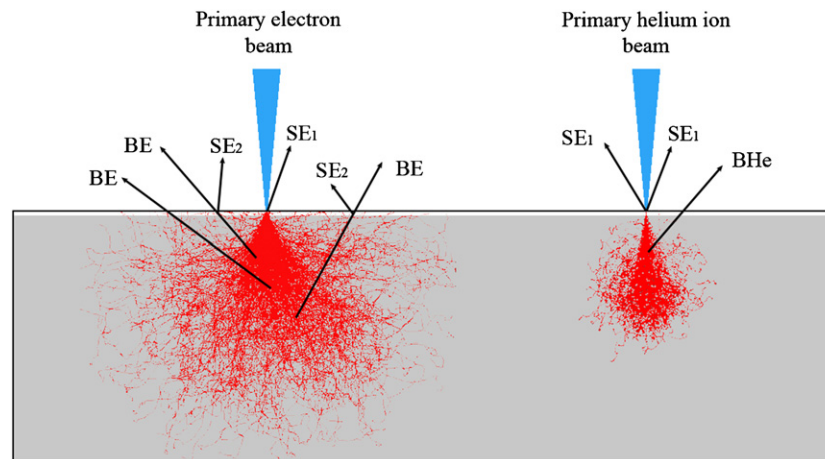
Figure 5. Diagrammatic representation of the contemporary understanding of the difference between the signal generating interactions in the SEM (left) and the HIM (right).

used extensively for resist patterning mainly because of the resolution constraints. However, HIM lithography with ~200 nm resolution was demonstrated over 20 years ago, but it suffered from a lack of adequate ion column technology to make it a viable competition to EBL [22]. One advantage to using helium ions for lithography is the potential for higher resolution lithography than electrons. The helium ion microscope has demonstrated that it is capable of generating extremely fine lines with extremely straight walls due to the deep penetration of the helium ions into the substrate and the lack of additional secondary exposure mechanisms which can degrade the lithographic fidelity. Winston *et al* [23] has shown dense arrays of approximately 15 nm diameter hydrogen silsesquioxane (HSQ) resist posts generated by helium ion lithography. HSQ is a high resolution electron beam resist and it permits high-resolution SEM inspection following patterning and development. The helium ion beam lithography technology is in its infancy but, it has already demonstrated an ability to fabricate less than 10 nm lines with a 20 nm pitch [23]. There is still much to be done, but ion beam lithography shows promise and the sensitivity of the resist materials can be substantially higher, so higher throughput lithography may be possible.

3.3. Enhanced surface detail

In both the SEM and HIM the size and shape of the excited and information volumes along with the SE generation efficiency and location are important for another reason. The amount of surface-related information collected is directly dependent on these factors. Those SE carrying information about the finest details of the sample are generated by the primary electrons or ions at the point where the beam hits the sample. These are the so-called SE-1 type electrons. The SEs that were created by energetic electrons or ions backscattered within the sample are designated as SE-2 electrons. Because of the location of their generation in the SEM, the SE-2 do not carry information about finest sample details; in fact, it is clearly shown in figure 5 (left) that current modeling shows that many more electrons emerge remotely from the initial point of the

primary electron interaction than shown in the modeled data from the ion beam. The consequence of this is a reduction of contrast of the fine structure. The size of this area depends on the primary excitation and the material composing the sample under examination and can extend more than a micrometer in diameter [24]. Electrons can also be generated by the backscattered electrons or ions that leave the sample and hit some other material within the sample chamber or the sample itself. These SEs are called SE-3. Again, these do not carry information about finest sample details. What is not shown in figures 4 and 5 is the additional cascade of SEs generated by these interactions which may magnify this by a factor of 3 to 5 times.

The well-focused beam always generates SE-1, but the relative amounts of SE-1, SE-2 and SE-3 electrons generated in total have a profound effect on the appearance and the amount of fine details resolved in the SE image. Peters [25] measured the individual contributions of the components of the SE signal (in the SEM) from gold crystals and found that, depending upon the sample viewed, for the total SE image, the contribution of the SE-2 is approximately 30% and the contribution to the image of the SE-3 electrons is approximately 60% as compared with approximately 10% of the image contributed by the SE-1 derived signal. This ratio of SE-2/SE-1 generated by electrons significantly reduces the contrast and resolvability of small features. Clearly, this depends on landing energy, the SE and backscattered electron or ion yields.

In the HIM, SEs forming the image are produced at (or very near) the point of initial interaction with the sample, and thus are equivalent to SE-1 electrons of the SEM (figure 5). The initial SEs produce images with strong and topographic contrast, and generally appear very similar to the SE images obtained from an SEM, upon first inspection. IONiSE modeling [26, 27] predicts that the helium-ion-generated SE-2/SE-1 ratio should be lower than that for electron irradiation especially at the higher landing energies. Hence, the contrast and the surface details are enhanced. In contrast to the SEM interactions, the ion beam passes much more deeply into the sample matrix (figure 5) and very few SE-2 or SE-3 type electrons that can dominate in the SEM imaging are
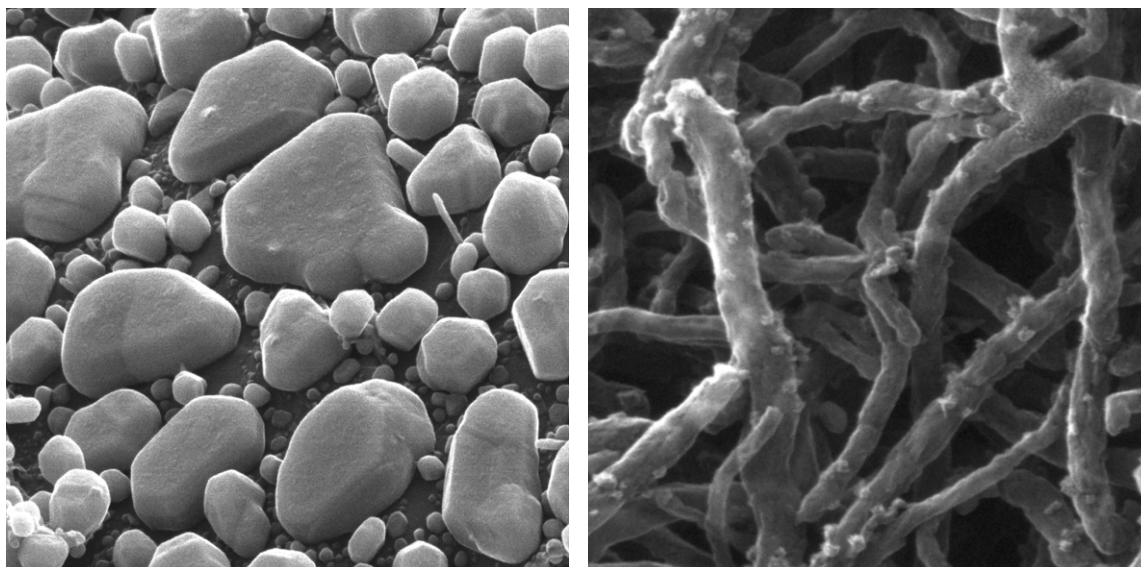
Figure 6. HIM imaging and surface structure enhancement. (Left) typical gold-on-carbon image test sample viewed in the HIM (field of view = 1.5 μm). Note that surface detail is being resolved on the top surface of the gold islands which would not be typically observed in a similar SEM image. (Right) carbon nanotube material with tin and palladium nanoparticles on or near the surface (field of view = 500 nm).

generated. The flood of SE-2 and SE-3 electrons resulting from the backscatter of electrons in the SEM can essentially 'wash-out' some of the surface detail potentially resolved by the electron beam. This does not occur to the same extent in the HIM, resulting in the enhanced surface detail as shown in figure 6. Thus, in a material infinitely thicker than the SE escape depth, clear surface detail may be resolved.

A flat sample is instructive, but dimensional metrology is the measurement of a structure of some sort. Structures have edges and we usually make measurements from one 'edge' to another edge such as the diameter of a gold particle, or the critical dimension of a semiconductor device gate. Edges are also found at grain boundaries and material interfaces. If an edge is introduced at the point of primary beam incidence, depending upon the angle selected, the collected signal can be generated from points down the slope of that structure where the excited volume approaches the surface. All signals generated are summed for that particular pixel. This explains the bright edges on the typical SEM image. For accurate metrology, understanding all of the interactions involved in the signal generation process is extremely important in order to obtain meaningful dimensional information because the size of the edge 'bloom' in the SEM is often larger than the desired measurement accuracy.

Due, in part, to the huge difference between the electron and ion interaction volume and the reduction of SE-2, and SE-3 electrons, it is clear that a fundamental difference in the signal-to-noise ratio between the SEM and the HIM is possible. Peters demonstrated that up to 90% of the collected SEM signal is composed of electrons generated remotely from the initial impact of the primary electron beam [25]. Hasselbach and Möllenstedt [24] also showed experimentally using the emission microscope that the collected signal from the SEM could be generated from adjacent structures micrometers from the primary beam impact point. In comparison, in

the HIM, the collection of the equivalent of SE-2 and SE-3 signals is greatly minimized because their signal contribution is formed too deeply in the material for them to escape. Edge enhancement in the HIM still occurs, but is a function of the structure size relative to the ion beam penetration and scatter. Hence, the main contributors to the total HIM image are the SE-1 electrons. It stands to reason that in the HIM, the amount of signal collected under similar conditions to the SEM should differ, as well as the contrast of the surface structure. Measurement of these differences is an area of research at the current time, and as more is known these thoughts may be refined. But, what is clear is that fine detail on the surface of a sample such as in figure 6 (left) will appear more readily in the HIM since the other signal mechanisms potentially 'washing-out' the fine detail in the SEM are minimized.

Sub-surface contributions to the SEM image are common and can also be found in the HIM image. In very thin materials, low in atomic number or those that are flocculent, significant contributions to the image can be made from underlying structures (figure 6 right). The SEM or HIM beam enters the first layer of the sample, generates signal and then passes through (potentially generating signal as well). As it strikes another adjacent fiber or portion of the sample, it also generates signal [11]. The sum of both is collected by the SE detector. This effect can be seen on some of the carbon nanotubes in figure 6 (right) where a sub-surface 'ghosting' occurs. Other possible mechanisms for generating the sub-surface signal in bulk samples include electron channeling effects. Further research into these mechanisms and the underlying physics needs to be done in order to understand fully these observations. For now, adjusting instrument operating conditions helps to minimize these contributions.

Modeling is an excellent tool for understanding the physics of electron and ion interactions. NIST has devoted a great deal of effort to modeling and has a long history
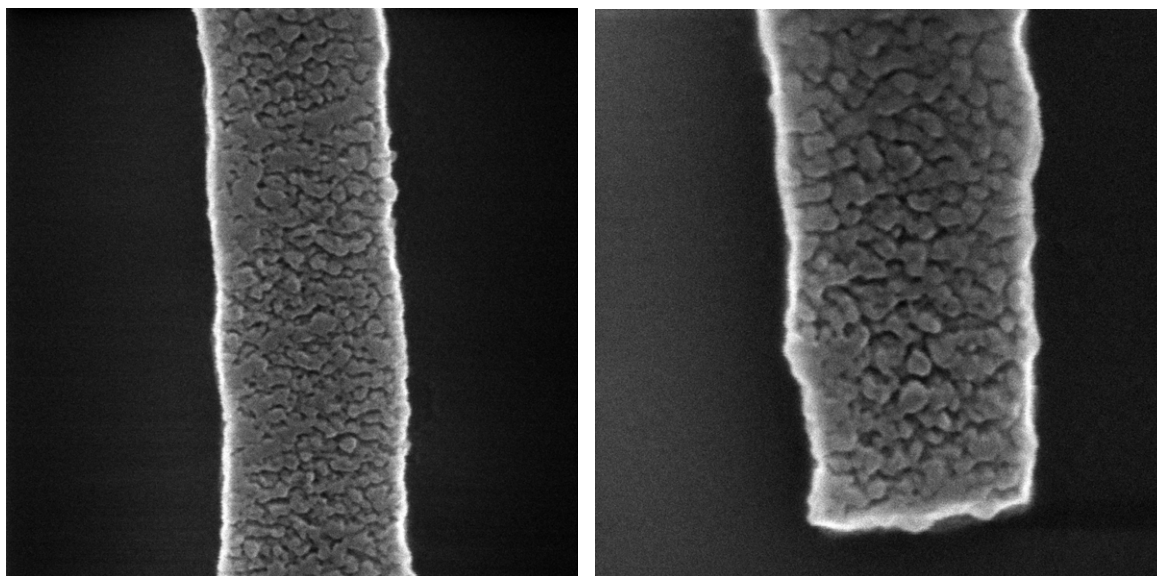
Figure 7. Imaging of uncoated chromium on glass photomasks by incorporating the electron flood gun to eliminate positive charge build-up. (Field of view = 700 nm, left; 500 nm, right.)

in this area. The most recent improvements in the NIST program JMONSEL are documented by Villarrubia *et al* [28, 29]. Villarrubia *et al* (2007) detail how 3D shapes are described and how a scattering calculation is made [28]. Villarrubia *et al* (2009) describe subsequent improvements to the physics model and the relationship between the models one uses and the resulting measurement values (e.g., for positions of a feature's edges) [29].

3.4. Signal collection

Measurements made in particle beam instruments are made from the collected signal chosen (secondary electron, backscattered electron, transmitted electron, etc). It must be understood that the signal measured is a complex product of (a) the interaction of the electron or ion probe with the sample, (b) the composition of the sample, (c) the sample chamber geometry and chamber material, (d) the type of detector used, and (e) the electro-magnetic fields present around the sample (either from the instrument itself or from sample biasing and/or charging). Where the critical dimension metrology SEM (CD-SEM) is concerned many of these parameters are fixed, and nearly 'identical' samples are viewed on a day-by-day basis. Because of this tight control, a very high degree of precision can be obtained. However, accuracy is a different issue [30]. Sophisticated modeling methods that account for all the physical processes must be used to measure accurately the shape and size of the sample structures of interest [13]. Monte Carlo models have been in use at NIST to deconvolute the edge information from the collected signal, and those models are being modified to accommodate the signal generated in the HIM. Work is ongoing to combine the physics of the IONiSE Monte Carlo model [26, 27] with the 3D shape modeling of JMONSEL [28, 29] and will aid in the prediction of topographic yield variation of the helium generated SE as a function of the sample composition and structure shape. With this model, the important details of

helium ion SE imaging can be compared with comparable electron-generated SE imaging. Such work is an important and primary step in the understanding of the imaging and metrology of the HIM.

3.5. Charge reduction

Current HIM instruments operate routinely at high accelerating voltages. Many samples being viewed can build up a positive charge on the surface. Unlike the SEM, where the negative charge build-up can be quite high, high enough to detrimentally deflect the electron beam in some instances, the positive charging in the HIM can be eliminated or at least minimized by employing an electron flood gun. Operating conditions can be established to facilitate viewing nonconducting materials such as photoresist or biological samples.

The electron flood gun is also useful in imaging and metrology of insulating materials such as chromium on quartz photomasks. Photomasks can be very difficult to image in the SEM due to charge build-up in the quartz. Postek *et al* (2003) successfully used variable pressure SEM to dissipate the charge build-up for the imaging and metrology of chromium photomasks [31]. The HIM can also be successfully employed in the imaging and metrology of these samples (figure 7). The positive charge build-up was removed by employing an electron flood gun, thus enabling high resolution imaging of the chromium photomasks. Optimization of the electron flood gun is currently being undertaken to determine the proper conditions for common semiconductor materials and the effects of this tool upon measurements (such as beam deflection) made while it is being operated.

3.6. Helium ions

Current theory is that most of the He ions remain embedded in the sample due to the low backscattered ion coefficient for He.
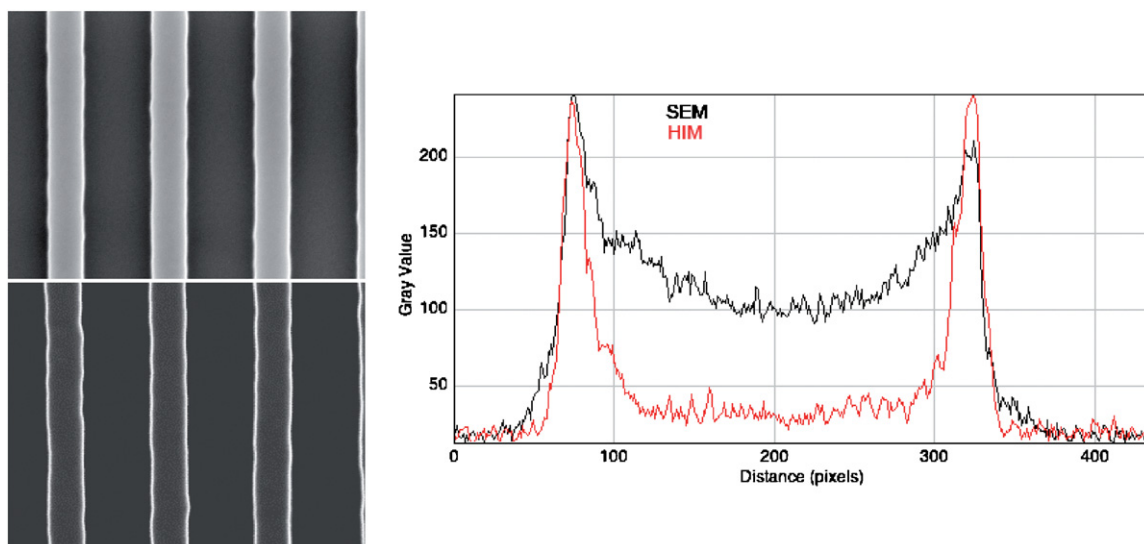
Figure 8. Comparison of SEM and HIM. (Left) typical SEM and HIM images of polysilicon structures (field of view of 3 μm). Note the difference in contrast and edge definition. (Right) comparison of linescans of conductive patterned amorphous silicon lines and the complementary SEM (upper line) and HIM images (lower line) exhibiting similar characteristics.

The ions may cause swelling, formation of tiny bubbles, and in certain cases diffuse out of the sample. For many practical cases and primary ion currents, the effects of the embedded He ions are negligible, and do not prevent high-resolution imaging. The images in this and other publications attest to this. The effect of the He ions on sensitive samples is currently being researched.

4. Semiconductor imaging and metrology

The potential of achieving higher resolution and greater surface sensitivity has prompted a great deal of interest in the HIM for semiconductor metrology applications. The SEM is currently the tool of choice for semiconductor production, and sample charging is often an issue. Many samples in the SEM are prone to charging, and charge reduction is commonly achieved by lowering the accelerating voltage down into the 1 kV range to achieve a charge balance [32]. The immediate result has, historically been, a significant reduction in resolution due to beam broadening. Hence, edge definition is also broadened. Modeling has been able to deconvolute edge information from the images, but requires an accurate model to be used in conjunction with a well-characterized instrument. Aberration corrected SEMs working at low accelerating voltage may, in the near future, improve upon this situation and this avenue is also being explored currently.

Semiconductor metrology with the HIM is different (today) in that most of the commercial HIMs operate at high electron landing energies, and a variable accelerating voltage option is just being implemented in on these instruments in the field. Therefore, no quantitative comparisons of the HIM and the SEM at a low landing energy have been published. Figure 8 shows a comparison of linescans of conductive patterned amorphous silicon lines. These are complementary SEM (figure 8, upper) and HIM images (figure 8, lower). The images (and linescans) were both taken at high landing

energies and thus provides highly distinct edge definition as shown in the figure. But, note that the contrast range in the HIM image is much greater. Thus, allowing more flexibility in the measurement algorithm selection and the number of data points used in the measurement. In addition, the edge sharpness would be expected to be much higher than that of the low accelerating voltage SEM. Additional work to understand the proper conditions for semiconductor metrology with the HIM is ongoing.

The HIM benefits from the difference in specimen interaction to provide higher surface detail. Modeling of the ion beam interaction has shown that in the helium ion microscope, the general characteristics of the measurement profile are similar to those obtained from the SEM. Earlier work on x-ray mask structures [33] in the SEM with transmission electron detection demonstrated for the first time a 'notch' structure apparent in the modeled linescan. This notch is a consequence of the electron beam generating signal as it scans along the sidewall. The finer the beam and better the resolution, the more distinct is the notch. More recent modeling has shown this to be a characteristic of the SEM signal generation and now the HIM. Similarly, the modeling may relate to the time that the ion beam resides on the sidewall of the structure under test. But, since the HIM is potentially higher in resolution, this characteristic may be more pronounced. The inflection point is thought to be reproducible and as such is being closely looked at as a possible fiducial to the location of the structure edge. This may ultimately lead to an accurate measurement even without the benefit of modeling but with some degree of measurement uncertainty still to be determined. Currently, work in this area is also being pursued.

4.1. HIM for semiconductor production applications

As stated above, the HIM is being considered for online and off-line metrology applications. Hence, a series of preliminary studies were done to to assess the potential of this technology
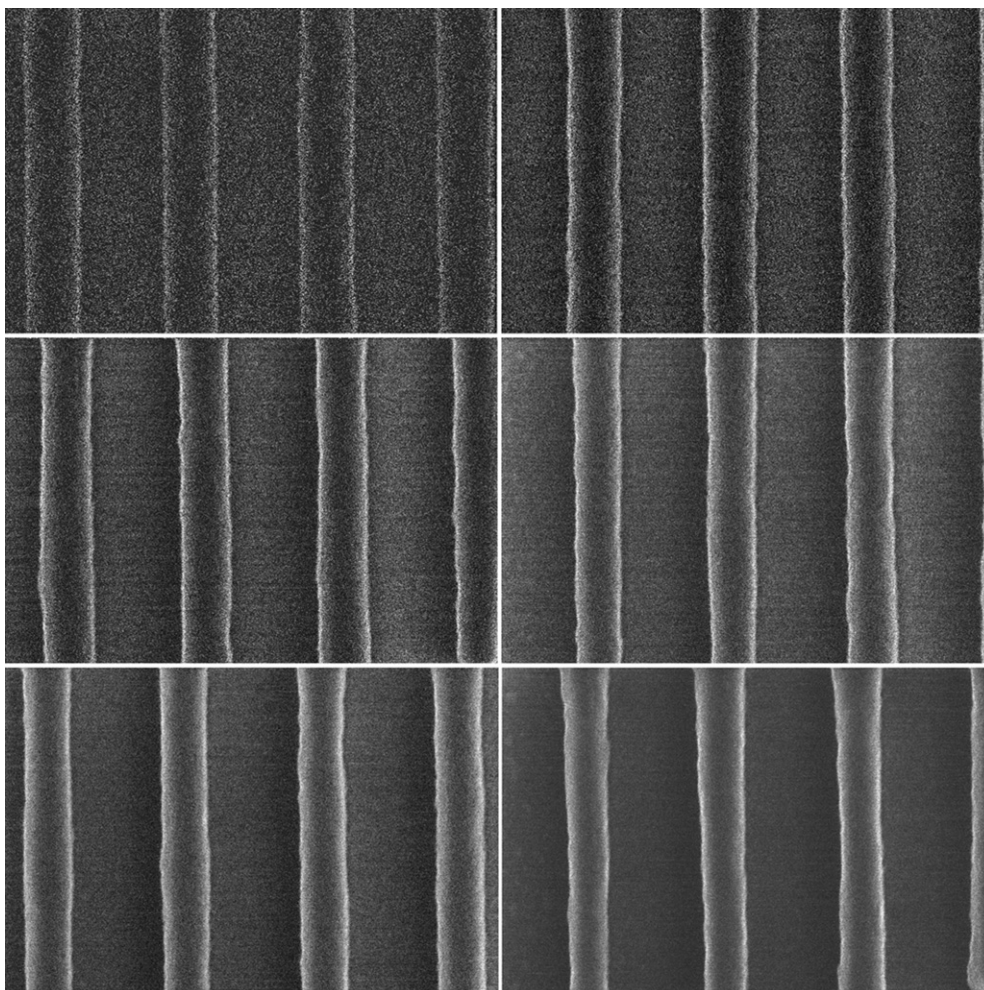
Figure 9. Series of HIM slow scan image showing the progression in image quality by differing only the pixel dwell time, as described in the text. (Top, left) 0.5 μs; (top, right) 2.0 μs; (middle, left) 5.0 μs; (middle, right) 10.0 μs; (bottom, left) 20.0 μs; (bottom, right) 40.0 μs. Note the improvement in the signal-to-noise ratio, but the slimming of the lines in the longer dwell times and the poorer signal-to-noise ratio in the shorter dwell times (field of view = 1 μm).

for these purposes. The work includes (1) the basic imaging configurations to assess signal-to-noise conditions, (2) resist damage section comparing performance of the HIM for two different resist systems currently being used in semiconductor lithography, (3) application of a measure of the apparent beam reporting on a resolution measure that is in common use in the semiconductor industry [34–37], and (4) an assessment of the HIM for cross section imaging mode.

4.1.1. Imaging for metrology. Patterned photoresist structures are highly sensitive to electron and ion irradiation, thus it is essential to use the minimum beam exposure dose to accomplish the metrology task without damaging the material. On the other hand, too few SEs collected per pixel introduce unacceptable shot noise-induced error in the determination of feature edge location. A compromise between dose and measurement signal-to-noise must be achieved. Figure 9 shows a series of six slow scan images which differ only in the pixel dwell time. Dwell times range from 0.5 to 40 μs per pixel. Slow scan imaging refers to capturing the image by performing a single pass of the beam in raster fashion over the

structure at a rate given by the pixel size divided by the dwell time. All high magnification imaging in these studies used a 1 nm pixel size.

The images in the series show a steady progression in image quality where the 0.5 μs dwell time image shows speckling due to low SE count per pixel while the 40 μs image is remarkably free of this effect. These images were captured by scanning only one time at a fresh location at the stated dwell time. There is a noticeable reduction in linewidth for the longest dwell times. This effect is referred to as 'line slimming'. From a metrology perspective the larger dwell times cause too much damage. But, the shorter dwell times result in the greater the noise, the greater the potential measurement errors (the next section makes these observations more quantitative).

It is appropriate to point out that all particle beam instruments can induce damage on a sample under test. The SEM had over 30 years of instrument experience behind it before uncoated photoresist samples were routinely viewed in semiconductor production. So, it should be noted that the HIM is a relatively new instrument, so a great deal is still
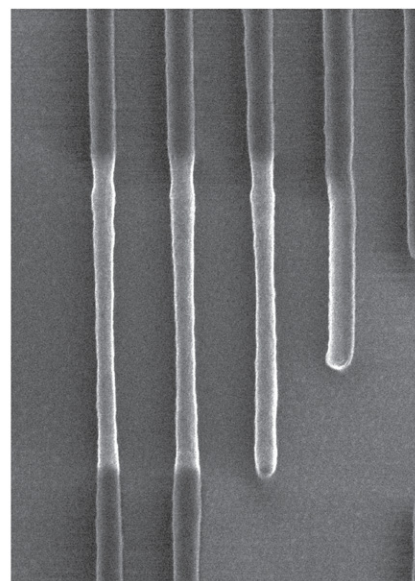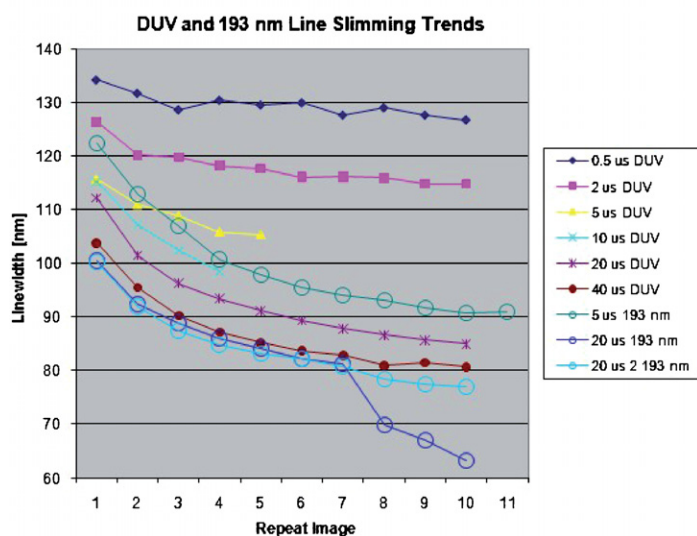
Figure 10. (Left) graphical analysis showing the full collection of slimming trends from the experiments as discussed in the text. (Right) HIM image showing the line slimming effect due to helium ion exposure (field of view = 2 μm).

to be learned about the proper operating parameters for these samples and many others.

4.1.2. Resist damage experiment. To test the effect of the helium ion beam on patterned photoresist, the basic experiment was to move and to find a fresh site on the photoresist and acquire ten images using the same imaging conditions for each data set. Immediately prior to acquiring the ten images, the beam astigmatism was minimized on a nearby structure. Image sets were then acquired for several different dwell times for the two resist types. Linewidth measurements of the same center line in each image set were performed using a standard commercial measurement software package [38].

The graphical analysis shown in figure 10 (left) shows the full collection of the line slimming trends from the experiments. Closed symbols are 248 nm DUV resist sample results and open symbols show 193 nm resist trends. Slimming trends for the 193 nm resist system were conducted only at 5 and 20 μs dwell times. These trends followed the behavior seen for the 248 nm resist system. There appears to be an intriguing edge brightening phenomenon that is present in all the image sets but is more pronounced for the higher dwell times; repeated images show systematically brighter edges. The HIM with which this work was done did not have automatic gain control, so during the first run on the 193 nm resist sample for a 20 μs dwell time, the detector amplifier went into saturation after seven repeats. These beam conditions were then repeated on a fresh site using a lower amplifier gain setting. The two series are shown in the figure and there is excellent reproducibility of the trend up to the point of amplifier saturation for the first set. Clearly, all of these data show a true slimming trend with helium ion beam exposure.

Additional experiments were conducted using the DUV samples. They all show that at short dwell time (0.5 μs) the slimming trend is linear with a slope of a few nanometers

per repeat. It is clear, however, that there is scatter of a few nanometers in the data about the linear trend. This scatter is an indication of the precision of the measurement for these beam conditions. At longer dwell times, the slimming trend is more pronounced and nonlinear. Figure 10 (right) shows a lower magnification image of the site where the ten 40 μs dwell time exposures were conducted. Slimming and edge brightening are clearly evident. The observations suggest that at low dwell time (0.5 μs or less), modest damage and reasonable precision is achievable. These data and subsequent experiments have shown that as the dwell time increases the measured linewidth decreases. These experiments are another indication that the proper metrology regime needs to be fully researched and short dwell times are currently recommended.

4.1.3. Apparent beam width. It is clear, from the previous discussions, that the term 'instrument resolution' is a complex function of a number of factors with both the instrument and sample playing the key roles. The determination of 'resolution' is more complicated than just laying a ruler on a micrograph and measuring the distance between two points. This concept is more involved than either the classical light microscope or even the TEM. In this instance, the specimen plays a major part in the overall performance measure. Clearly, instrument performance is a major issue and vast improvements in instrument design have strongly contributed to advances over the years in both SEMs and now the evolution of the HIM. Improved lens designs and illumination sources have been the main contributors to the increased SEM instrument performance. But, instrument resolution relies not only on a high performing instrument design and instrument operating conditions, but also on the material being viewed to demonstrate successfully the performance characteristics. Particle beam interactions and also the nature and manner of the signal being collected are major contributors. Hence, sample choice plays a significant role in demonstrating the
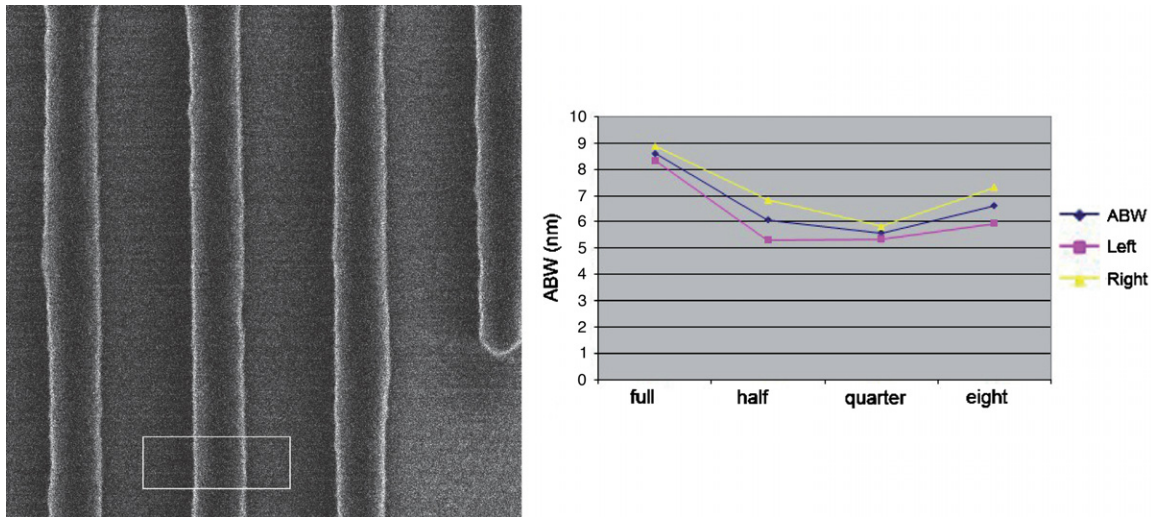
Figure 11. Apparent beam width. (Left) HIM image acquired on the DUV sample using a relatively small dwell time (field of view = 1 μm) and analyzed by averaging all the rows of pixels within the box shown at the bottom of the middle line as discussed in the text.

performance of these instruments. It is also likely that the perceived instrument resolution for each sample will vary depending upon the materials composing that particular sample. For that reason, specialized samples have been developed for the demonstration of resolution capabilities. These samples have had to evolve as did the instruments. But, one must always keep in mind that one sample may work better than another for a particular set of operating conditions or instrument design, so one must be continually vigilant that fair evaluations are made. In order to minimize this issue, the semiconductor manufacturing has adopted the concept of apparent beam width or ABW [34–37]. ABW represents a rough measure of the edge location uncertainty. The idea is to use a typical measurand in semiconductor manufacturing such as a photoresist line (as in these experiments) and determine the edge width using common topographic locations. Providing that the edge profile is vertical or even undercut, the edge has been shown to be a sensitive measure of 'resolution' under imaging conditions appropriate for metrology of that particular material or structure [34–37]. When the edge profile is not ideal, this measure overestimates the true ABW. ABW accounts for the instrument performance and the effects of the sample, thus providing a comparative measure of the instrument performance (as long as the measurement parameters are kept constant).

Figure 11 (left) shows a HIM image acquired on the DUV sample using a relatively short dwell time to minimize the effects of slimming. Using the NIH ImageJ software [39] the image was analyzed by averaging all the rows of pixels within the box shown at the bottom of the middle line. This box represents approximately one-eighth of the full lines in the image. The process is repeated for larger boxes covering one-quarter, one-half, and the full vertical extent of the image. The reduction in noise on these waveforms as the box size increases is the result of averaging more and more rows of the image. The left and right edge widths are calculated by finding the distance between the edge peak maximum intensity location and the location where the outside falling

edge intercepts the baseline. The ABW is the average of the two edge widths. The left and right edge widths along with the ABW are plotted in figure 11 (right) as a function of area averaged or box height. These data goes through a shallow minimum with the ABW slightly less than 6 nm. This behavior can be understood as resulting from a competition between two opposing trends: as the box size decreases, the noise in the waveform increases which tends to broaden the edge peak and increase the calculated edge widths. On the other hand, as the box size increases, miss-alignment of the line edges from vertical tends to broaden the average peaks in the waveform. So for these various reasons, the value of 6 nm ABW for the HIM under the beam conditions for this test is considered an upper estimate. In comparison, the corresponding ABW for a CD-SEM, measured under similar sample conditions, is typically significantly larger, closer to 9 nm. This is a impressive result for the HIM. However, it should be noted that the typical operation of a production CD-SEM is at low voltage.

4.1.4. Imaging for cross section analysis. Cross section imaging and metrology of patterned photoresist is very important to semiconductor manufacturing. It is very difficult to characterize the shape at the foot of the photoresist for subsequent steps from only a top-down SEM or HIM view. A HIM image of a sample of the 193 nm patterned and developed photoresist was cleaved through the nested line feature and is shown in figure 12. This figure clearly shows important sidewall details such as the standing waves produced by the interference of incoming and reflected light during the photolithography process. What is remarkable is a confirmation of the significant DOF in the image. As previously described in figure 2, there are diagonal breaks in the lines every 5 μm. These breaks are clearly seen for the first several repetitions down the tilt plane beyond the cleave. At these magnifications, it is unusual to see this combination of crisp near field detail and deep DOF from SEM's designed and used for cross section metrology.
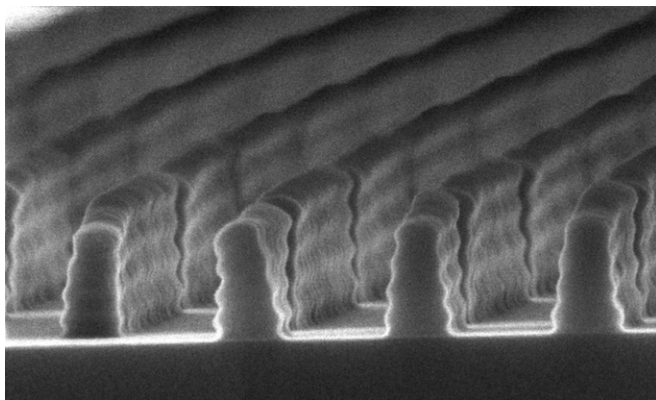
Figure 12. HIM image of a sample of the 193 nm patterned and developed photoresist cleaved through the nested line feature showing important sidewall details such as the standing waves produced by interference of incoming and reflected light during the lithography process (field of view = 1 μm). Note the significant depth of field shown in the image.

5. Helium ion beam milling and sample damage

The potential for ion beam-induced sample damage is discussed in several sections of this paper. Some level of change ('damage') in the sample is inevitable during any type of work with particle beam instrumentation. The point is what type of changes occur and to what extent. This depends a great deal upon sample, landing energy and dose, and pre-treatment of the material being imaged or measured and the particle being used. This varies widely in both the SEM and HIM. Sample damage can be greater in the HIM than the SEM because the ions have much higher momentum than electrons of the same energy—and the difference is larger still when you take into account that SEM is typically operated at lower energy than HIM. It is up to the skilled operator to choose the optimal setting and imaging conditions to minimize the change, and for the metrology be able to properly account for it. In some instances the damage is detrimental and should be avoided and in some instances it can be exploited such as for nano-milling.

Depending upon the beam current, the flux of particles within the excited volume of either the SEM or the HIM can be substantial. As shown earlier (section 4.1.2) this current can lead to sample degradation [8]. Moreover, much of the energy of the primary electrons or ions may stay within the sample, which can cause additional adverse effects such as sample melting, swelling or other dimensional changes. Figure 13 is an image showing an example of the potential for high precision material removal from a sample using the HIM. This illustrates the effects of irradiation of approximately 3 pA beam current for approximately 60 s at 28 keV ion landing energy on an evaporated gold island. In figure 13, the instrument conditions were changed from imaging to a very small scanned region (very high magnification image setting) for material removal. The small square region at the 2 o'clock location has also been removed earlier through irradiation with the helium ion beam. In this figure, the small 10 nm hole was intentionally milled near the center of the gold island in point irradiation
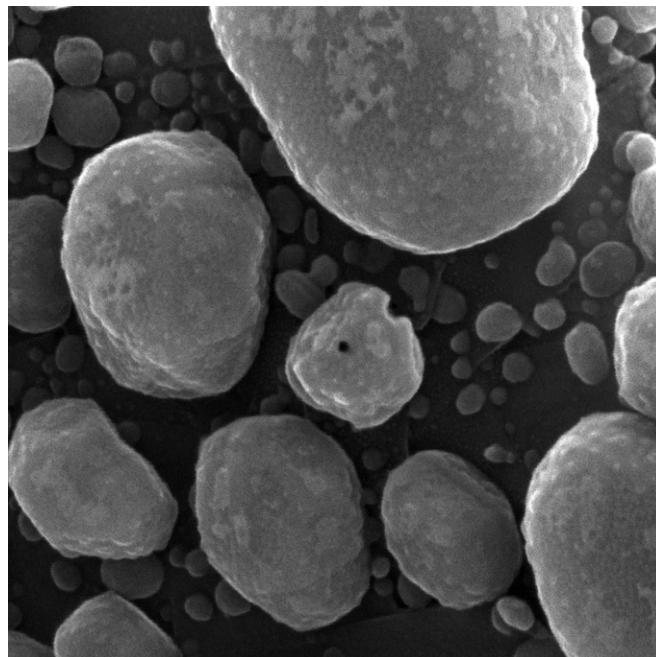

Figure 13. Image of a gold on carbon sample showing the precision milling possible with the HIM. A notch was removed from the gold island as well as a small 10 nm hole milled near the center of the island (field of view = 800 nm).

mode thus, showing how precisely the beam can be positioned and material removed. The HIM can also be used for more extensive material removal (or addition) in a similar manner to the gallium focused ion beam microscope.

5.1. Sample contamination

Electron beam-induced sample contamination is a classic concern for SEM and HIM imaging and metrology. This is another form of specimen damage. Controlling specimen contamination in the SEM has been discussed elsewhere [40, 41] and has direct application to the HIM. The high surface sensitivity of the HIM (discussed earlier) makes it even more susceptible to sample contamination than the SEM. This is due to the effect of the ion beam and the resulting SEs on the thin layer of molecules of water and carbon dioxide on the sample or oily residues, either from the stage fabrication process or lubricants. Radio frequency (RF) plasma cleaning [42] has been shown to virtually eliminate sample contamination in the SEM and has been incorporated in the HIM with equal success.

6. Conclusions

A significant and rapid evolution of the HIM instrumentation has occurred for imaging and metrology. Since its introduction, the performance of the instrument has markedly improved, as well as the attainable resolution [12, 14]. Typically, the benchmark of performance for scanned beam instruments is the measure of resolution. But, as discussed earlier, resolution determination is more complicated than just laying a ruler on a micrograph and measuring the distance between two points. Shown in this paper has been the

significant part the specimen plays in the overall measurement and hence instrument performance. Clearly, instrument performance is a strong issue and vast improvements in instrument design have strongly contributed to advances over the years in both SEMs and now the evolution of the HIM.

Research to enable accurate measurements in the HIM is ongoing. This work has documented that the resolution and DOF of this instrument can be better than the SEM. Equally, this work demonstrates that sample damage is a concern which must be overcome. Sample 'slimming' is an effect that must be understood and accommodated for both imaging and metrology. The experiments shown here show that valuable data can be obtained when this effect is properly recognized. Proper conditions for metrology with the HIM must be developed and this will take a good deal of work to explore the numerous possible operating conditions. Such work was needed for the SEM, and over time these conditions were found and it became a useful 'tool' for semiconductor manufacturing. Similar research is needed for the HIM.

Modeling of the HIM signal, just like the SEM signal, is crucial to the measurement capability and much progress has been made in that area which will ultimately lead to accurate measurements. However, as demonstrated in this work, precise measurements in either the SEM or the HIM can be accomplished as long as one is careful. As time progresses and more is understood about the imaging mechanisms in the HIM through experimentation and modeling, the advantages or disadvantages of this new instrument will become more apparent for nanometrology.

Acknowledgments

References

[1] Interagency Working Group on Manufacturing 2008 R&D Workshop Report *Instrumentation, Metrology and Standards for Nanomanufacturing* available at www.manufacturing.gov

[2] National Nanotechnology Initiative 2006 NNI Grand Challenge Workshop Report *Instrumentation and Metrology* available at www.nano.gov

[3] Postek M T and Lyons K 2007 Instrumentation, metrology, and standards key elements for the future of nanomanufacturing *Proc. SPIE* **6648** 664802

[4] National Nanotechnology Initiative 2010 NNI Affiliated Workshop *Cross-industry Issues in Nanomanufacturing Workshop Report* available at www.nano.gov

[5] Joy D C, Griffin B, Notte J, Stern L, McVey S, Ward B and Fenner C 2007 Device metrology with high-performance scanning ion beams *Proc. SPIE* **6518** 65181L

[6] Postek M T, Vladár A E, Kramar J, Stern L, Notte J and McVey S 2007 Helium ion microscopy: a new technique for semiconductor metrology and nanotechnology *Frontiers of Characterization and Metrology for Nanoelectronics* ed D G Seiler *et al* (New York: AIP) pp 161–7

[7] Postek M T, Vladár A E and Ming B 2009 Breaking the resolution barrier: understanding the science of helium ion beam microscopy *Frontiers of Characterization and Metrology for Nanoelectronics* ed D G Seiler *et al* (New York: AIP) pp 249–60

[8] Postek M T and Vladár A E 2008 Helium ion microscopy and its application to nanotechnology and nanometrology *Scanning* **30** 457–62

[9] Reiche R, Kaesmaier R, Rosenkranz R, Ritter U, Teichert S and Leinert S 2009 Applications of helium ion microscopy in semiconductor manufacturing *Microsc. Anal.* **23** 11–4

[10] Scopioni L, Sanford C A, Notte J, Thompson B and McVey S 2009 Understanding imaging modes in the helium ion microscope *J. Vac. Sci. Technol.* B **27** 3250–5

[11] Postek M T, Howard K S, Johnson A J and McMichael K 1980 *Scanning Electron Microscopy: A Student Handbook* (Burlington, VT: Ladd Research Industries)

[12] Vladár A E, Postek M T and Ming B 2009 On the subnanometer resolution of scanning electron and scanning helium ion microscopes *Microsc. Today* **3** 6–13

[13] Postek M T 1997 The scanning electron microscope. *Handbook of Charged Particle Optics* ed J Orloff (New York: CRC Press) pp 363–99

[14] 2009 Helium ion microscopy press release *Microsc. Anal.* **94** (Jan) 28

[15] Ward B, Notte J and Economou N 2006 Helium ion microscope: a new tool for nanoscale microscopy and metrology *J. Vac. Sci. Technol.* B **24** 2871–5

[16] Hovington P, Drouin D and Gauvin R 1997 CASINO: a new era of Monte Carlo code in C language for the electron beam interaction: part I. Description of the program *Scanning* **19** 1–14

[17] Drouin D, Hovington P and Gauvin R 1997 CASINO: a new era of Monte Carlo code in C language for the electron beam interaction: part II. Tabulated values of Mott cross section *Scanning* **19** 20–8

[18] Drouin D, Couture A R, Joly D, Tastet X, Aimez V and Gauvin R 2007 CASINO V2.42: a fast and easy-to-use modeling tool for scanning electron microscopy and microanalysis users *Scanning* **29** 92–101

[19] Ziegler J 1972 SRIM (Stopping and Range of Ions in Matter) software (http://www.srim.org/)

[20] Everhart T E and Chung M S 1972 Idealized spatial emission distribution of secondary electrons *J. Appl. Phys.* **43** 3707–11

[21] Everhart T E and Hoff P H 1971 Determination of kilovolt electron energy dissipation versus penetration distance in solid materials *J. Appl. Phys.* **42** 5837–46

[22] Horiuchi K, Itakura T and Ishikawa H 1988 Fine pattern lithography using a helium field ion source *J. Vac. Sci. Technol.* B **6** 241–4

[23] Winston D, Cord B, Ming B and Bell D 2009 Scanning-helium-ion-beam lithography with hydrogen silsesquioxane resist *J. Vac. Sci. Technol.* B **27** 2702–6

[24] Hasselbach F, Rieke U and Straub M 1983 An imaging secondary electron detector for the scanning electron microscope *Scann. Electron. Microsc.* II 467–78

[25] Peters K-R 1985 Working at higher magnifications in scanning electron microscopy with secondary and backscattered electrons on metal coated biological specimens and imaging macromolecular cell membrane structures *Scanning Electron Microsc.* **1985** 1519–44

[26] Ramachandra R, Griffen B and Joy D C 2008 Modeling for metrology with a helium beam *Proc. SPIE* **6922** 69221W

[27] Ramachandra R, Griffen B and Joy D C 2009 A model of secondary electron imaging in the helium ion scanning microscope *Ultramicroscopy* **109** 748–57

[28] Villarrubia J S, Ritchie N W M and Lowney J R 2007 Monte Carlo modeling of secondary electron imaging in three dimensions *Proc. SPIE* **6518** 65180K

[29] Villarrubia J S and Ding Z J 2009 Sensitivity of scanning electron microscope width measurements to model assumptions *J. Micro/Nanolith. MEMS MOEMS* **8** 033003

[30] Larrabee R D and Postek M T 1993 Precision, accuracy uncertainty and traceability and their application to submicrometer dimensional metrology *Solid-State Electron.* **36** 673–84

[31] Postek M T and Vladár A E 2003 Application of high pressure/environmental SEM microscopy for photomask dimensional metrology. Application of high pressure/environmental SEM microscopy for photomask dimensional metrology *CP 683 Characterization and Metrology for ULSI Technology: Int. Conf.* ed D Seiler *et al* (New York: AIP)

[32] Postek M T 1984 Low accelerating voltage inspection and linewidth measurement in the scanning electron microscope *Scan. Electron Microsc.* III 1065–74

[33] Postek M T, Lowney J R, Vladár A E, Keery W J, Marx E and Larrabee R D 1993 X-ray lithography mask metrology: use of transmitted electrons in an SEM for linewidth measurement *J. Res. Natl. Inst. Stand. Technol.* **98** 415–45

[34] Archie C N, Lowney J R and Postek M T 1999 Modeling and experimental aspects of apparent beam width as a resolution measure *Proc. SPIE* **3677** 699–85

[35] Mayer J A, Huizenga K, Solechy E, Archie C, Banke G, Cogley R, Nathan C and Robert J 2003 New apparent beam width artifact and measurement methodology for CDSEM resolution monitoring *Proc. SPIE* **5038** 699–710

[36] Deleporte A G, Allgair J, Archie C, Banke G, Postek M T, Schlesinger J, Vladár A E and Yanof A 2000 Benchmarking of advanced CD-SEM's against the new unified specification for sub-0.18 micrometer lithography *Proc. SPIE* **3998** 12–27

[37] Bunday B, Bishop M and Allgair J 2004 Results of benchmarking of advanced CD-SEMs at the 90 nm CMOS technology mode *Proc. SPIE* **5375** 151–72

[38] Metrologia—Spectel Research (http://www.spectelresearch.com/)

[39] NIH Image (http://rsb.info.nih.gov/nih-image/)

[40] Vladár A E, Postek M T and Vane R 2001 Active monitoring and control of electron-beam-induced contamination *Proc. SPIE* **4344** 835–43

[41] Vladár A E, Purushotham K P and Postek M T 2008 Contamination specification for dimensional metrology SEMs *Proc. SPIE* **6922** 692217

[42] Evactron—XEI Scientific (http://www.evactron.com)